Reduced Step Edges on Rutile TiO$_2$(110) as Competing Defects to Oxygen Vacancies on the Terraces and Reactive Sites for Ethanol Dissociation

U. Martinez, J. Ø. Hansen, E. Lira, H. H. Kristoffersen, P. Huo, R. Bechstein, E. Lægsgaard, F. Besenbacher,
B. Hammer,[†] and S. Wendt[*]

*Interdisciplinary Nanoscience Center (iNANO), Department of Physics and Astronomy, Aarhus University,
DK-8000 Aarhus C, Denmark*

The rutile TiO$_2$(110) surface is the most studied surface of titania and considered as a prototype of transition metal oxide surfaces. Reactions on flat TiO$_2$(110)-(1×1) surfaces are well studied, but the processes occurring on the step edges have barely been considered. Based on scanning tunneling microscopy studies, we here present experimental evidence for the existence of O vacancies along the $\langle 1\bar{1}1\rangle_R$ step edges (O$_S$ vac.'s) on rutile TiO$_2$(110). Both the distribution of bridging O vacancies on the terraces and temperature-programed reaction experiments of ethanol-covered TiO$_2$(110) point to the existence of the O$_S$ vac.'s. Based on experiments and density functional theory calculations, we show that O$_S$ vac.'s are reactive sites for ethanol dissociation via O-H bond scission. Implications of these findings are discussed.

The use of TiO$_2$-based materials for catalytic and photocatalytic applications has spurred tremendous research efforts [1–4]. At a fundamental level, surface science studies have often addressed the rutile TiO$_2$(110)-(1 × 1) surface, which has become a model of transition metal oxide surfaces [4–8]. However, the vast majority of these studies have focused on extended atomically flat terraces with bridging oxygen vacancies (O$_{br}$ vac.'s), whereas processes occurring at step edges have barely been explored [9]. Because many applications of TiO$_2$ are related to TiO$_2$ nanoparticles [1–4], the study of step edges and related extended topological defects is essential for an improved fundamental understanding of the reactivity of TiO$_2$ surfaces.

The rutile TiO$_2$(110)-(1 × 1) surface consists of alternating rows of fivefold coordinated Ti atoms and protruding, twofold coordinated O$_{br}$ atoms. The Ti atoms underneath the O$_{br}$ atoms are sixfold coordinated (6f-Ti), as any other Ti atom in stoichiometric rutile. Ar$^+$ sputtered and vacuum-annealed TiO$_2$(110) crystals are n-type semiconductors because of bulk defects such as Ti interstitials, O vacancies, and crystallographic shear planes [5,10–13]. Depending on the sample preparation protocols, TiO$_2$(110) surfaces with different average terrace widths and O$_{br}$ vac. densities can be prepared [14–16]. In the following, clean reduced TiO$_2$(110) surfaces with O$_{br}$ vac.'s are denoted as r-TiO$_2$(110).

Two types of step edges are dominating on r-TiO$_2$(110) surfaces: $\langle 001 \rangle$ and $\langle 1\bar{1}1 \rangle$ step edges [5,12,14,16–19]. Whereas the structure of $\langle 001 \rangle$ steps is today still unresolved, a stable reconstruction of the $\langle 1\bar{1}1 \rangle$ step edge (denoted as $\langle 1\bar{1}1 \rangle_R$) has been predicted recently, based on density functional theory (DFT) calculations [9]. Compared to bulk truncated $\langle 1\bar{1}1 \rangle$ step edges, this structure

is characterized by one additional TiO$_2$ unit per step unit cell [see light gray (yellow) dots in Fig. 1(a)]. The $\langle 1\bar{1}1 \rangle_R$ step edges are characterized by 5f- and 6f-Ti atoms, with the Ti's of the additional TiO$_2$ units being sixfold coordinated. Another important prediction put forward in Ref. [9] is that the $\langle 1\bar{1}1 \rangle_R$ step edges on r-TiO$_2$(110) are reduced. As shown in Fig. 1(b), O$_S$ vac.'s, i.e., O vacancies at the step edges, were found to be located at the end of the O$_{br}$ rows [9]. So far, no experimental evidence of these O$_S$ vac.'s has been reported.

In this Letter, we provide experimental evidence for the existence of O$_S$ vac.'s along the $\langle 1\bar{1}1 \rangle_R$ step edges on r-TiO$_2$(110) surfaces. Based on scanning tunneling microscopy (STM) measurements, we conducted a detailed analysis of the distribution of O$_{br}$ vac.'s on the r-TiO$_2$(110) surface, revealing that much fewer O$_{br}$ vac.'s exist in the vicinity of $\langle 1\bar{1}1 \rangle_R$ step edges than on the terraces. However, when O$_S$ vac.'s along the $\langle 1\bar{1}1 \rangle_R$ step edges are introduced, the total number of vacancies per surface area is constant.
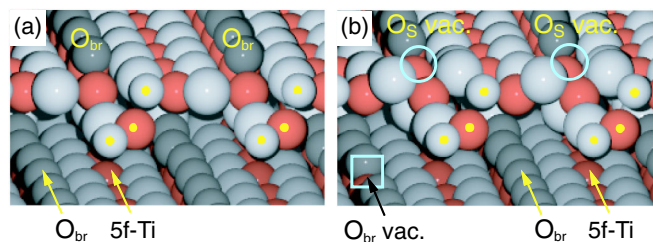
FIG. 1 (color online). (a) Stoichiometric TiO$_2$(110) surfaces with reconstructed $\langle 1\bar{1}1 \rangle_R$ step edges, i.e., with additional TiO$_2$ units. (b) Reconstructed $\langle 1\bar{1}1 \rangle_R$ step edge on r-TiO$_2$(110), characterized by O$_S$ vac.'s. Light gray (yellow) dots indicate additional TiO$_2$ units. In (b), O$_{br}$ vac.'s and O$_S$ vac.'s are indicated by squares and circles, respectively.

In addition, our combined approach of temperature-programed desorption or reaction (TPD/TPR) experiments and DFT calculations addressing ethanol (EtOH) exposed r-TiO$_2$(110) surfaces also reveals the existence of O$_S$ vac.'s.

Figure 2 shows empty-state STM images acquired from three different regions of a r-TiO$_2$(110) surface at 120–140 K [20]. The imaged 410 Å × 410 Å areas on the surface span several terraces that are labeled by Roman numbers; the uppermost terraces are marked by "I" and the lowest by "IV," respectively. On the surface of the same crystal, regions with low [Fig. 2(a)], medium [Fig. 2(b)], and high [Fig. 2(c)] step densities were identified. Even though the O$_{br}$ rows are geometrically protruding, they appear dark in the STM images, and the 5f-Ti atoms in the troughs bright [5]. Accordingly, the O$_{br}$ vac.'s on the terraces appear as bright spots on dark lines in high-resolution STM [see the inset of Figs. 2(b) and 2(d)].

To test whether a correlation exists between extended defects such as step edges and O$_{br}$ vac.'s, we counted the O$_{br}$ vac.'s in different regions on the r-TiO$_2$(110) surface, where the abundance of $\langle 1\bar{1}1 \rangle_R$ steps varied. In total, we extracted the number of O$_{br}$ vac.'s from 17 STM images of 410 Å × 410 Å size characterized by total $\langle 1\bar{1}1 \rangle_R$ step length between 60 and 140 nm [gray (red) bars in Fig. 2(e)]. Additionally, we analyzed ten 130 Å × 130 Å STM images showing areas without any steps [hatched bar in Fig. 2(e)]. We found that the number of O$_{br}$ vac.'s per 410 Å × 410 Å area varies considerably between ~618 and ~815, implying that the O$_{br}$ vac.'s are inhomogeneously distributed on the r-TiO$_2$(110) surface.

Next, we included the $\langle 1\bar{1}1 \rangle_R$ step edges in our analysis. Specifically, we extracted from the STM images the number of $\langle 1\bar{1}1 \rangle_R$ step sites, here defined as the number of O$_{br}$ rows terminating at $\langle 1\bar{1}1 \rangle_R$ step edges [Fig. 2(e), dark gray (blue) bars]. It is evident that the sum of O$_{br}$ vac.'s and $\langle 1\bar{1}1 \rangle_R$ step sites per surface area is constant and that the number of O$_{br}$ vac.'s is high in regions with few $\langle 1\bar{1}1 \rangle_R$ steps and low in regions with many step sites. In fact, when plotting the number of O$_{br}$ vac.'s against the number of $\langle 1\bar{1}1 \rangle_R$ step sites [Fig. 2(f)], the slope is $-(0.93 \pm 0.16)$, suggesting one O$_S$ vac. per $\langle 1\bar{1}1 \rangle_R$ step site. Thus, by introducing the O$_S$ vac.'s along the $\langle 1\bar{1}1 \rangle_R$ step edges, we arrive at a situation where the total number of O vac.'s is independent of the step density in the STM images. Therefore, we take our results as a strong indication that the $\langle 1\bar{1}1 \rangle_R$ step edges are reduced, i.e., that the O$_S$ vac.'s do indeed exist.

Interestingly, we observed a depletion of O$_{br}$ vac.'s in the vicinity of the $\langle 1\bar{1}1 \rangle_R$ step edges [see Fig. 2(d)]. Specifically, on the upper terraces of the $\langle 1\bar{1}1 \rangle_R$ steps, a ~20 Å wide zone exists, within which almost no O$_{br}$ vac.'s occur. The $\langle 1\bar{1}1 \rangle_R$ step edges and O$_{br}$ vac.'s can be considered as competing defects on the surfaces of bulk-reduced TiO$_2$(110) crystals. In contrast, no clear correlation was found between the number of O$_{br}$ vac.'s and $\langle 001 \rangle$ step sites. Accordingly, to provide a precise measure of the surface reduction (total surface O vac. density, ρ_T), the $\langle 1\bar{1}1 \rangle_R$ step edges need to be taken into account. Two procedures are possible to determine a precise measure of the surface reduction: (i) exclusively STM images acquired on flat terraces are analyzed, or (ii), when regions spanning several terraces were scanned, each $\langle 1\bar{1}1 \rangle_R$ step site is counted as one O$_S$ vac. For the data presented in

FIG. 2 (color online).   (a)–(c) Selected STM images (410 Å × 410 Å) showing areas of (a) low, (b) medium, and (c) high total step length, all acquired from the same r-TiO$_2$(110) surface [20]. In (a), black and white arrows indicate $\langle 1\bar{1}1 \rangle_R$ and $\langle 001 \rangle$ step edges, respectively. The inset in (b) shows a 82 Å × 82 Å large zoom-in on a terrace. (d) Zoom-in STM image (82 Å × 82 Å) of the area indicated in (b). Squares indicate O$_{br}$ vac.'s. (e) Number of O$_{br}$ vac.'s [gray (red) bars] and $\langle 1\bar{1}1 \rangle_R$ step sites [dark gray (blue) bars] of 17 STM images (410 Å × 410 Å) acquired on different regions on r-TiO$_2$(110). Bars corresponding to the STM images depicted in (a)–(c) are indicated. The hatched gray (red) bar on the left shows the number of O$_{br}$ vac.'s in ten 130 Å × 130 Å areas located far from any step edges. The total area of these ten areas almost equals that of the 17 410 Å × 410 Å STM images. The dashed line indicates the average sum of O$_{br}$ vac.'s and $\langle 1\bar{1}1 \rangle_R$ step sites. (f) Number of O$_{br}$ vac.'s plotted against the number of $\langle 1\bar{1}1 \rangle_R$ step sites corresponding to the data shown in (e).

Fig. 2, both procedures led to $\rho_T = (9.2 \pm 0.5)\%$ ML on all scanned regions on the surface, where 1 ML is the density of the (1×1) unit cells, 5.2×10^{14} cm^{-2}. However, if the $\langle 1\bar{1}1 \rangle_R$ step sites were ignored, the surface reduction would be underestimated by up to 25%.

To further our studies addressing the presence of O_S vac.'s at the $\langle 1\bar{1}1 \rangle_R$ step edges, we utilized EtOH as a probe and conducted combined STM and TPD/TPR experiments (Fig. 3). Two sets of experiments were conducted with the same TiO$_2$(110) crystal as used for the STM experiments presented above, but the surface reduction was with ρ_T(O vac.) = $(7.4 \pm 0.2)\%$ ML lower. Following EtOH exposures at $\sim$270 K (saturation), we flashed the samples to 380 and 570 K, respectively, to selectively remove different types of ethoxide species from the surface.

On terraces of r-TiO$_2$(110) surfaces, three different EtOH-related species are known: molecularly and dissociatively adsorbed EtOH on top of $5f$-Ti atoms (EtOH$_{Ti}$ and EtO$_{Ti}$, respectively) and ethoxides adsorbed at O$_{br}$ vac.'s (EtO$_{br}$) that result from EtOH dissociation via O-H bond scission at the O$_{br}$ vac.'s [21–23]. H adatoms (H$_{ad}$ species) are formed upon dissociation of EtOH both in the Ti troughs and in the O$_{br}$ vac.'s. After flashing the sample to 380 K ("experiment I") exclusively, EtO$_{br}$ ethoxides and H$_{ad}$ species are expected to remain on the terraces [21–23], but the STM data presented in Fig. 3(a) show that adsorbates also persisted along the $\langle 1\bar{1}1 \rangle_R$ step edges [see Fig. 3(a), inset (ii)]. This important result confirms the

presence of O$_S$ vac.'s because, according to our TPD/TPR and DFT results presented below, trapping sites are required to stabilize any EtOH-related species on the r-TiO$_2$(110) surface so strongly. In analogy to the EtO$_{br}$ ethoxides on the terraces, we ascribe the adsorbates along the step edges as ethoxides, EtO$_S$. The EtO$_S$ ethoxides are located at the end of O$_{br}$ rows, and their coverage is close to 1. After flashing the sample to 570 K [see Fig. 3(b), "experiment II"], our STM analysis revealed that exclusively the EtO$_{br}$ species remained on the surface, whereas the EtO$_S$ ethoxides at the $\langle 1\bar{1}1 \rangle_R$ step edges disappeared. Furthermore, we observed that O$_{br}$ vac.'s appeared on the surface [see Fig. 3(b), insets (i) and (ii)], indicating that H$_{ad}$ species recombined upon flashing to 570 K, which led to the formation of O$_{br}$ vac.'s on the surface and water that desorbed [24,25].

The TPD/TPR spectra corresponding to these experiments [Fig. 3(c)] confirm that the species adsorbed along the $\langle 1\bar{1}1 \rangle_R$ step edges are ethoxides. The TPD/TPR experiments reveal the desorption of ethylene (C$_2$H$_4$, $m/e = 26$) and EtOH ($m/e = 31$), as is expected for the reaction of ethoxide species via β-hydride elimination [21,22]. In the TPD/TPR spectra corresponding to "experiment I," two distinct C$_2$H$_4$ peaks exist at $\sim$500 K (β) and $\sim$640 K (γ), respectively, whereas, in the TPD/TPR spectra corresponding to "experiment II" [Fig. 3(c)], only the γ-C$_2$H$_4$ peak at $\sim$640 K was detected. The desorption of C$_2$H$_4$ is accompanied by the desorption of water [26].
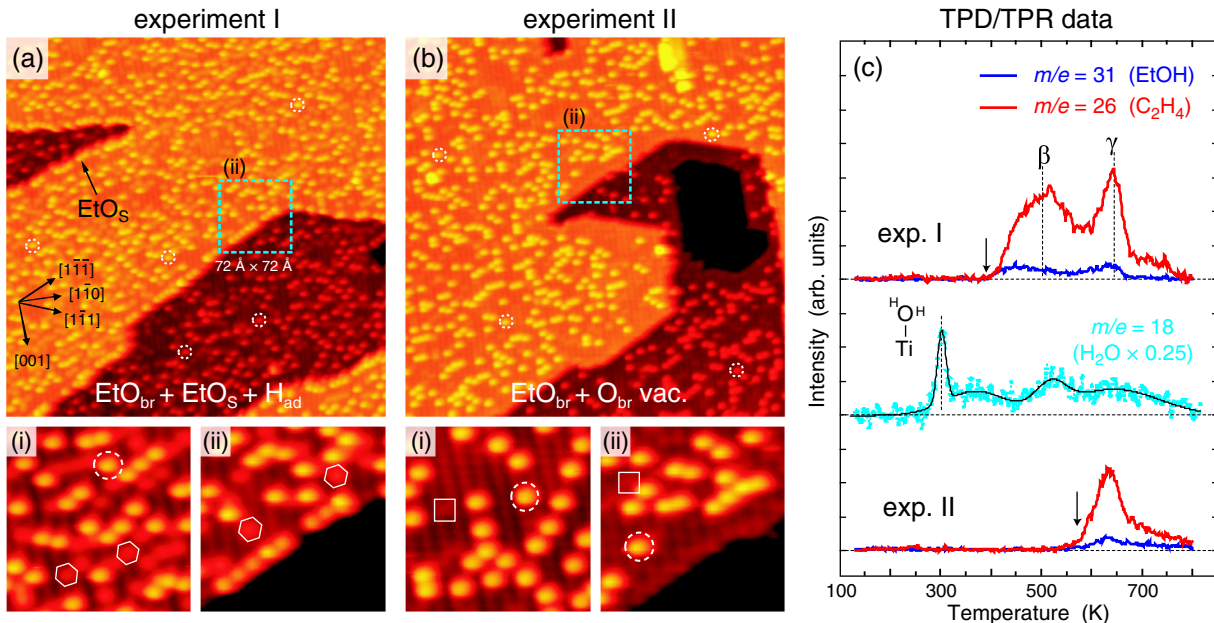
FIG. 3 (color online).   STM images (390 Å $\times$ 390 Å) of EtOH/r-TiO$_2$(110) prepared by saturating r-TiO$_2$(110) surfaces with EtOH at 270 K and flashing to (a) 380 K and (b) 570 K, respectively [20]. Insets (i) were acquired from other areas on the two surfaces. Insets (ii) are enlargements of the areas indicated in (a) and (b), respectively. All insets show areas of 72 Å $\times$ 72 Å. Symbols indicate EtO$_{br}$ ethoxides (dotted circles), H$_{ad}$ species (hexagons), and O$_{br}$ vac.'s (squares), respectively. (c) Corresponding TPD/TPR experiments with $m/e = 26$ (C$_2$H$_4$) and $m/e = 31$ (EtOH) traces. EtOH cracking fragments to the $m/e = 26$ signal were substracted. For "experiment I," the $m/e = 18$ signal (H$_2$O) is also shown (scaled by 0.25). Black arrows in (c) indicate the flashing temperatures.
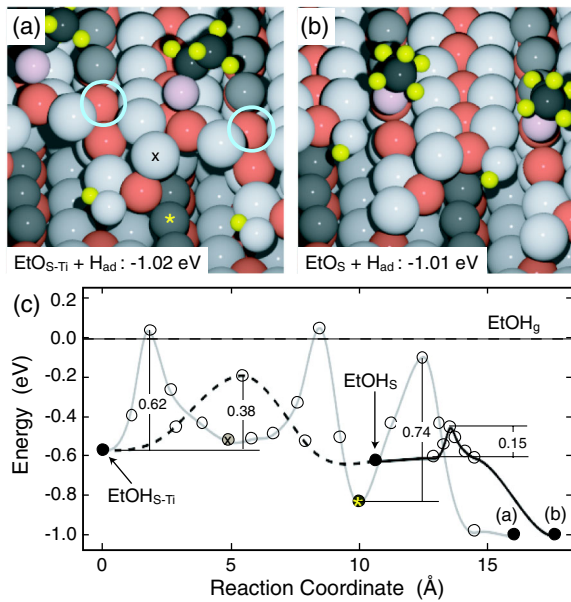
FIG. 4 (color online).   Computed most stable EtOH adsorption structures at reduced $\langle 1\bar{1}1 \rangle_R$ step edges. (a) Dissociatively adsorbed EtOH at the end of the Ti troughs, consisting of EtO_{S-Ti} and H_{ad} species. (b) Dissociatively adsorbed EtOH at the end of the O_{br} rows, consisting of EtO_S and H_{ad} species. Atoms of the adsorbates are shown as follows: C atoms: dark gray (black) balls; O atoms: large light gray (pink) balls; H atoms: small light gray (yellow) balls. Circles indicate O_S vac.'s. (c) Potential energy curves of EtOH at reduced $\langle 1\bar{1}1 \rangle_R$ step edges. The solid light gray curve describes the dissociation of $EtOH_{S-Ti}$ to EtO_{S-Ti} and H_{ad} species, with the two local minima corresponding to configurations where the H_{ad} species are adsorbed on the O atoms indicated in (a). The dashed black curve describes the diffusion of $EtOH_{S-Ti}$ into an O_S vac. and the solid black curve its subsequent dissociation. Potential energies are with respect to EtOH in the gas phase ($EtOH_g$).

The data presented in Fig. 3 suggest that the two distinct C_2H_4 features at ~500 K (β) and ~640 K (γ) observed in "experiment I" arise from β-hydride elimination of EtO_S and EtO_{br} ethoxides, respectively. The different line shape of the two C_2H_4 peaks and the rather large integrated area of the β-C_2H_4 peak indicate possible diffusion events to be involved in the C_2H_4 formation between 400 and 570 K. Even though the C_2H_4 formation reactions may be complex, it is clear that the EtO_{br} ethoxides are more stable on the surface than the EtO_S ethoxides.

In our DFT calculations at the generalized gradient approximation level [20], we started with the step structure proposed in Ref. [9] that is characterized by O_S vac.'s [see Fig. 1(b)]. EtOH molecules may bind at the $\langle 1\bar{1}1 \rangle_R$ step edges either on top of a $5f$-Ti atom ($EtOH_{S-Ti}$) or directly in an O_S vac. ($EtOH_S$). For both sites, EtOH molecules are rather weakly bound with ~0.5 eV. The dissociation of an $EtOH_{S-Ti}$ molecule, forming EtO_{S-Ti} ethoxides and H_{ad} species [Fig. 4(a)], is hindered by a substantial barrier, 0.62 eV, and further along the dissociation path an even higher energy barrier of 0.74 eV appears [see the solid light gray line in

Fig. 4(c)]. Given the fact that these barriers are higher than the adsorption energy of ~0.5 eV, $EtOH_{S-Ti}$ molecules would rather desorb than dissociate. This means that the species seen in the STM images along the step edges [Fig. 3(a)] cannot be explained by $EtOH_{S-Ti}$ molecules. On the contrary, the dissociation of an $EtOH_S$ molecule is hindered by a very low barrier of 0.15 eV, which can be easily overcome [see the solid black line in Fig. 4(c)]. Upon dissociation via O-H bond scission, an EtO_S ethoxide and a H_{ad} species are formed at the end of the O_{br} row [Fig. 4(b)]. The configuration shown in Fig. 4(b) is expected experimentally because the diffusion of $EtOH_{S-Ti}$ molecules from $5f$-Ti sites into the O_S vac.'s is facile [see the dashed black line in Fig. 4(c)]. For this diffusion process, the barrier was computed to be 0.38 eV, which is comparable to the diffusion of $EtOH_{Ti}$ molecules along the Ti troughs (~ 0.4 eV [23,27]). Compared to the EtO_{br} ethoxy species, which binds with an adsorption energy of ~1.5 eV [23], the EtO_S species are by ~0.5 eV less strongly bound and their adsorption energy is ~1 eV. Thus, the O_S vac.'s are mild trapping sites of EtOH molecules. Accordingly, our DFT calculations are in line with the above TPD/TPR data, revealing that the EtO_S species react at lower temperatures than the EtO_{br} species.

The presented results, i.e., the inhomogeneous distribution of O_{br} vac.'s (Fig. 2), as well as the combined STM, TPD/TPR, and DFT data addressing the EtOH − r-TiO$_2$(110) interaction (Figs. 3 and 4), evidence the existence of the O_S vac.'s at the $\langle 1\bar{1}1 \rangle_R$ step edges. Consequently, when describing reactions on r-TiO$_2$(110) surfaces, the processes occurring at the $\langle 1\bar{1}1 \rangle_R$ step edges need to be considered as well, even though these processes are intricate to model. Furthermore, when describing r-TiO$_2$(110) surfaces by STM, the $\langle 1\bar{1}1 \rangle_R$ step edges need to be taken into account. Specifically, when comparing r-TiO$_2$(110) surfaces obtained on different crystals (and laboratories), the O_{br} vac. densities can only be used as a criterion of the sample reduction if regions close to step edges are omitted. Moreover, for a fair comparison, the step densities on the surfaces need to be considered.

*Corresponding author
swendt@phys.au.dk
†Corresponding author
hammer@phys.au.dk

[1] X. Chen and S. S. Mao, Chem. Rev. **107**, 2891 (2007).
[2] A. Fujishima, X. T. Zhang, and D. A. Tryk, Surf. Sci. Rep. **63**, 515 (2008).
[3] M. A. Henderson, Surf. Sci. Rep. **66**, 185 (2011).

[4] T. L. Thompson and J. T. Yates, Jr., Chem. Rev. **106**, 4428 (2006).

[5] U. Diebold, Surf. Sci. Rep. **48**, 53 (2003).

[6] C. L. Pang, R. Lindsay, and G. Thornton, Chem. Soc. Rev. **37**, 2328 (2008).

[7] S. Wendt *et al.*, Surf. Sci. **598**, 226 (2005).

[8] Z. Dohnálek, I. Lyubinetsky, and R. Rousseau, Prog. Surf. Sci. **85**, 161 (2010).

[9] U. Martinez, L. B. Vilhelmsen, H. H. Kristoffersen, J. Stausholm-Møller, and B. Hammer, Phys. Rev. B **84**, 205434 (2011).

[10] R. A. Bennett, Phys. Chem. Comm. **3**, 9 (2000).

[11] S. Wendt *et al.*, Science **320**, 1755 (2008).

[12] E. Lira, S. Wendt, P. Huo, J. Ø. Hansen, R. Streber, S. Porsgaard, Y. Y. Wei, R. Bechstein, E. Lægsgaard, and F. Besenbacher, J. Am. Chem. Soc. **133**, 6529 (2011).

[13] E. Lira *et al.*, Catal. Today **182**, 25 (2012).

[14] E. Lira, J. Ø. Hansen, P. Huo, R. Bechstein, P. Galliker, E. Lægsgaard, B. Hammer, S. Wendt, and F. Besenbacher, Surf. Sci. **604**, 1945 (2010).

[15] K. F. McCarty and N. C. Bartelt, Surf. Sci. **540**, 157 (2003).

[16] S. Bonanni, K. Ait-Mansour, W. Harbich, and H. Brune, J. Am. Chem. Soc. **134**, 3445 (2012).

[17] U. Diebold, J. Lehman, T. Mahmoud, M. Kuhn, G. Leonardelli, W. Hebenstreit, M. Schmid, and P. Varga, Surf. Sci. **411**, 137 (1998).

[18] R. E. Tanner, M. R. Castell, and G. A. D. Briggs, Surf. Sci. **412**, 672 (1998).

[19] R. Bechstein, H. H. Kristoffersen, L. B. Vilhelmsen, F. Rieboldt, J. Stausholm-Møller, S. Wendt, B. Hammer, and F. Besenbacher, Phys. Rev. Lett. **108**, 236103 (2012).

[20] The STM and TPD/TPR experiments were carried out in a UHV chamber equipped with a homebuilt variable-temperature Aarhus STM, a quadrupole mass spectrometer, and standard facilities for sample preparation and characterization [7,14]. All STM measurements were conducted
in the constant current mode (tunneling voltage $\sim +$1.25 V, tunneling current of ~ 0.1 nA) with the sample at 120–140 K. The DFT calculations were performed using the Perdew-Burke-Ernzerhof exchange correlation functional as implemented in the grid-based projector augmented wave (GPAW) program. Electrons were described using the projector augmented wave method in the frozen core approximation. The $\langle 1\bar{1}1\rangle_R$ step edges were modeled using vicinal rutile (451) surfaces in a $Ti_{59}O_{118}$(451) slab. See Supplemental Material at http://link.aps.org/supplemental/10.1103/PhysRevLett.109.155501 for experimental and computational details, additional STM images, and computed most stable EtOH adsorption structures.

[21] L. Gamble, L. S. Jung, and C. T. Campbell, Surf. Sci. **348**, 1 (1996).

[22] Y. K. Kim, B. D. Kay, J. M. White, and Z. Dohnálek, J. Phys. Chem. C **111**, 18 236 (2007).

[23] J. Ø. Hansen, P. Huo, U. Martinez, E. Lira, Y. Y. Wei, R. Streber, E. Lægsgaard, B. Hammer, S. Wendt, and F. Besenbacher, Phys. Rev. Lett. **107**, 136102 (2011).

[24] M. B. Hugenschmidt, L. Gamble, and C. T. Campbell, Surf. Sci. **302**, 329 (1994).

[25] M. A. Henderson, W. S. Epling, C. H. F. Peden, and C. L. Perkins, J. Phys. Chem. B **107**, 534 (2003).

[26] In addition to EtOH-related products, we found that H_2O desorbed from the surface at ~ 300, ~ 500, and ~ 640 K, respectively [Fig. 3(c), "experiment I"]. The peaks at ~ 500 and ~ 640 K arise from the recombinations of H_{ad} species that are created upon β-hydride elimination of ethoxides [21], and the H_2O peak at ~ 300 K originates from H_2O species in the Ti troughs [24,25] that adsorbed during scanning of the surface.

[27] P. Huo, J. Ø. Hansen, U. Martinez, E. Lira, R. Streber, Y. Y. Wei, E. Lægsgaard, B. Hammer, S. Wendt, and F. Besenbacher, J. Phys. Chem. Lett. **3**, 283 (2012).